A V-shape Photonic Crystal Fiber Polarization Filter Based on Surface Plasmon Resonance Effect

Yuwei Qu[a)] Jinhui Yuan[a)b)c)*] Xian Zhou[b)c)] Feng Li[c)] Chao Mei[a)] Binbin Yan[a)] Qiang Wu[d)] Kuiru Wang[a)] Xinzhu Sang[a)] Keping Long[b)] Chongxiu Yu[a)]

a State Key Laboratory of Information Photonics and Optical Communications, Beijing University of Posts and Telecommunications, Beijing 100876, China

b Research Center for Convergence Networks and Ubiquitous Services, University of Science & Technology Beijing (USTB), Beijing 100083, China

c Photonics Research Centre, Department of Electronic and Information Engineering, The Hong Kong Polytechnic University, Hung Hom, Hong Kong

d Department of Physics and Electrical Engineering, Northumbria University, Newcastle upon Tyne, NE1 8ST, United Kingdom

ABSTRACT In this paper, a V-shape photonic crystal fiber (PCF) polarization filter based on surface plasmon resonance (SPR) effect is proposed. With the full vector finite element method, the V-shape photonic crystal fiber polarization filter is designed, and the coupling characteristics between the core mode and surface plasmon polariton mode are analyzed. The simulation results show that the fiber parameters have significant effects on the shift and strength of the SPR wavelength. Moreover, the losses of the core modes along the Y and X polarization directions are 68904 dB/m and 858 dB/m at the SPR wavelength of 1550 nm, respectively. Finally, the extinction ratio and error-tolerant rate of extinction ratio are also analyzed. The proposed V-shape PCF polarization filter can achieve good filtering effect in the communication band and is easy to integrate with existing optical fiber communication and sensing systems.

Keywords Surface plasmon resonance; photonic crystal fiber; polarization filter; extinction ratio

1. Introduction

Since the surface plasmon resonance (SPR) effect and photonic crystal fiber (PCF) are respectively proposed[1-3], the SPR effect combined with PCF has attracted great research interests[4-6]. In 2007, Zhang et al. successfully fabricated the PCF with silver-coated air holes by chemical vapor deposition and analyzed the polarization characteristics of the PCF[7]. In 2008, Schmidt et al. reported that high-quality nanowire can be fabricated by inserting the molten metal rod to hollow channel of the PCF[8]. In the same year, Lee et al. introduced the gold nanowire into a birefringent PCF, which results in strong polarization-dependent transmission[9]. Such a fiber can be used as novel correlated filtering and polarization devices[10-12].

The fiber filter plays an important role in laser and optical communication systems Many researchers have designed a variety of polarization filters based on the mode coupling between the surface plasmon polariton (SPP) mode and guide-mode of the PCF. In 2013, Xue et al. designed a PCF filter with gold-coated air holes, where the propagation loss along the Y polarization direction was 508 dB/cm at 1310 nm[13]. In 2015, Jiang et al. designed a liquid core PCF filter with gold-coated air holes, where the propagation losses along the Y and X polarization directions were 536 dB/cm and 5.29 dB/cm at 1550 nm, respectively[14]. In 2018, Yang et al. designed a polarization filter of high-birefringence PCF selectively coated with silver layers[15]. In 2018,

Zhou et al. designed a novel offset core photonic crystal fiber filter based on surface plasmon resonance, where the loss along the Y polarization direction was 657 dB/cm at 1550 nm[16]. However, it is difficult to fabricate such a PCF filter due to the liquid-filled air hole and super-large air holes in the cladding region. In addition, the D-shape PCF filter is difficult to couple with other optoelectronic devices, which greatly limits its practicality.

In this paper, a V-shape PCF polarization filter based on the SPR effect is proposed. The mode coupling characteristics between the core mode and SPP mode are investigated. By optimizing the structure parameters, a polarization filter with a filter bandwidth of 130 nm across the C-band is obtained. The extinction ratio and error-tolerant rate of extinction ratio are also analyzed.

2. Design of the V-shape PCF Polarization Filter

The V-shape PCF polarization filter structure designed is shown in Fig. 1. The background material of the PCF is pure silica. The air holes are arranged in a V-shape. The hole-hole pitch is Λ, and the air hole diameters are d_1 and d_2, respectively. In the X direction, two large air holes with diameter d_3 are introduced to induce the birefringence. A gold film with a thickness of t was coated on the inner side of the air hole in the Y direction to excite the SPP mode.

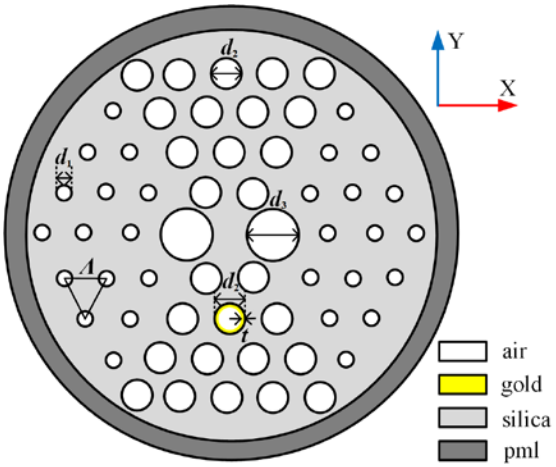

Fig. 1 Cross-section of the designed V-shape PCF polarization filter.

The full-vector finite element method is used to investigate the mode characteristics and calculate the effective refractive indices of the core mode and SPP mode of the PCF. The material dispersion of silica can be calculated by Sellmeier equation[17]. The relative dielectric constant of gold can be described by the Drude-Lorentz model[18]

$$\varepsilon_{\mathrm{m}} = \varepsilon_{\infty} - \frac{\omega_{\mathrm{D}}^2}{\omega(\omega - j\gamma_{\mathrm{D}})} - \frac{\Delta\varepsilon \cdot \Omega_{\mathrm{L}}^2}{(\omega^2 - \Omega_{\mathrm{L}}^2) - j\Gamma_{\mathrm{L}}\omega}, \tag{1}$$

where ε_{∞}=5.9673 is the high frequency dielectric constant, Δ_{ε}=1.09 is the weighted coefficient, ω is the angle frequency of the guided-wave, ω_{D} and γ_{D} are the plasma and damping frequency, and Ω_{L} and Γ_{L} represent the frequency and frequency bandwidth of Lorentz oscillator. Here, $\omega_{\mathrm{D}}/2\pi$=2113.6 THz，$\gamma_{\mathrm{D}}/2\pi$=15.92 THz，$\Omega_{\mathrm{L}}/2\pi$=650.07 THz，and $\Gamma_{\mathrm{L}}/2\pi$=104.86 THz.

In the calculation, a perfectly matching layer is introduced to absorb the radiation energy incident from different angles [19-21]. By dividing the solution domain into several triangular grids, the effective refractive index of the mode can be calculated. By using the imaginary parts of the effective refractive indices of the core and SPP modes, their confinement losses (L_{C}) can be

described as following[22]

$$L_C = \frac{20}{\ln 10}\frac{2\pi}{\lambda}\mathrm{Im}[n_{\mathrm{eff}}]\times 10^6, \tag{2}$$

3. Simulation Results and Discussion

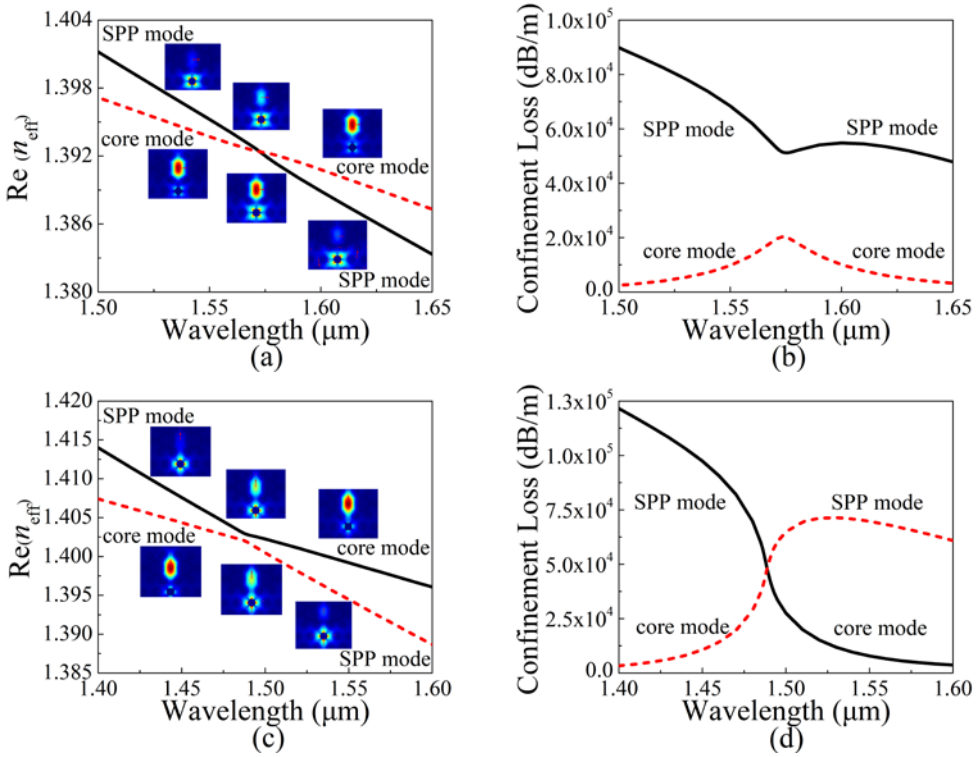

Fig. 2 (a) Effective refractive index real part Re(n_{eff}) and **(b)** confinement loss of the core mode and the second-order SPP mode along the X-polarization direction as functions of wavelength, and **(c)** Re(n_{eff}) and **(d)** confinement loss of the core mode and the second-order SPP mode along the Y-polarization direction as functions of wavelength. The insets of (a) and (c) show the mode field distributions of the core mode and second-order SPP mode at different wavelengths.

When the initial structure parameters are set as Λ=2.2 μm, d_1=0.9 μm, d_2=1.2 μm, d_3=2.5 μm, and t=50 nm, Re(n_{eff}) of the core mode (fundamental mode) and second-order SPP mode along the X-polarization direction as functions of wavelength are shown in Fig. 2(a). The insets of Fig. 2(a) show the mode field distributions of the core mode and second-order SPP mode at different wavelengths. From Fig. 2(a) and the insets, Re(n_{eff}) of the second-order SPP mode is larger at the shorter wavelength, and most of energy of the core mode and second-order SPP mode is bound to the core and surface of the gold film. At the longer wavelength, energy distributions of the core mode and second-order SPP mode are the same as those at the shorter wavelength, but Re(n_{eff}) of the core mode is larger than that of the second-order SPP mode. Re(n_{eff}) of the two modes has an intersection at wavelength 1573 nm, where is called as the resonant wavelength. At the resonant wavelength, energies of the core mode and second-order SPP mode mainly remain in the regions of the core and gold film surface, respectively. The weak energy transduction between the core mode and second-order SPP mode occurs, forming an incompletely coupled supermode. Fig. 2(b) shows the confinement loss curves of the core mode and second-order SPP mode. According to the coupled-mode theory [23], the confinement losses of the two modes are not equal, and there

are maximum and minimum at the resonant wavelength, respectively. Fig. 2(c) shows Re(n_{eff}) of the core mode and second-order SPP mode along the Y-polarization direction as functions of wavelength. Re(n_{eff}) of the two modes has an inverse intersection at resonant wavelength 1489 nm. The insets of Fig. 2(c) show the mode field distributions of the two modes at different wavelengths. From Fig. 2(c) and the insets, energy of the second-order SPP mode is mainly distributed on the gold film surface at the shorter wavelength. With the increase of wavelength, energy of the second-order SPP mode is gradually coupled from the gold film surface to the core region, and energy of the core mode is gradually coupled from the core region to the gold film surface. The energies of the core mode and second-order SPP mode occur to strong exchange at the resonant wavelength, forming a completely coupled supermode. At the resonant wavelength, energy of the core mode is the same as that of the second-order SPP mode. The confinement loss curves of the core mode and second-order SPP mode are shown in Fig. 2(d). Based on the coupled-mode theory, the confinement losses of the two modes are equal at the resonant wavelength.

The confinement losses of the core mode along the X-polarization and Y-polarization directions as functions of wavelength are shown in Fig. 3. From Fig. 3, the confinement losses increase first and then decrease with the increase of wavelength. The resonance wavelength of the core mode along the X-polarization direction is located at 1573 nm, where the maximum loss is 20250 dB/m. The resonance wavelength of the core mode along the Y-polarization direction is located at 1489 nm, where the maximum loss is 47189 dB/m. In contrast, the confinement loss of the core mode along the X- polarization direction is 1991 dB/m at 1489 nm. By comparison, at the resonance wavelength of 1489 nm, the confinement loss of the Y- polarization core mode is much higher than that of the X-polarization core mode. When the optical wave at wavelength 1489 nm is propagated, the Y-polarization core mode will decay rapidly and only the X-polarization core mode is remained. Thus, the filtering effect is achieved. In the following, we will focus on investigating the influences of the PCF structure parameters on the filtering effect.

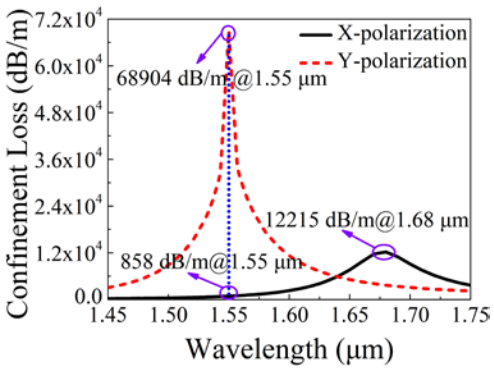

Fig. 3 Confinement losses of the X-polarization and Y-polarization core modes as functions of wavelength.

Figs. 4(a) and 4(b) show the confinement losses of the X-polarization and Y-polarization core modes of the V-shape PCF polarization filter with different *t*, respectively. With the increase of *t*, Re(n_{eff}) of the second-order SPP mode decreases, and Re(n_{eff}) of the core mode remains unchanged. From Fig. 4(a), the two modes along the X-polarization direction change from the incomplete to complete coupling, the resonance wavelength of the X-polarization core mode occurs to blue-shift, and the peak loss decreases first and then increases. From Fig. 4(b), the two modes along the Y-polarization direction achieve the complete coupling, the resonance

wavelength of the Y-polarization core mode occur to blue-shift, and the peak loss increases first and then decreases.

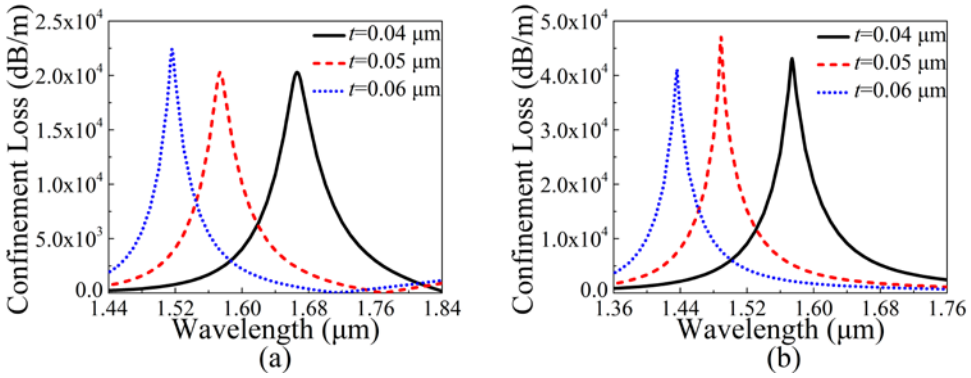

Fig. 4 The confinement losses of **(a)** X-polarization and **(b)** Y-polarization core modes for different t.

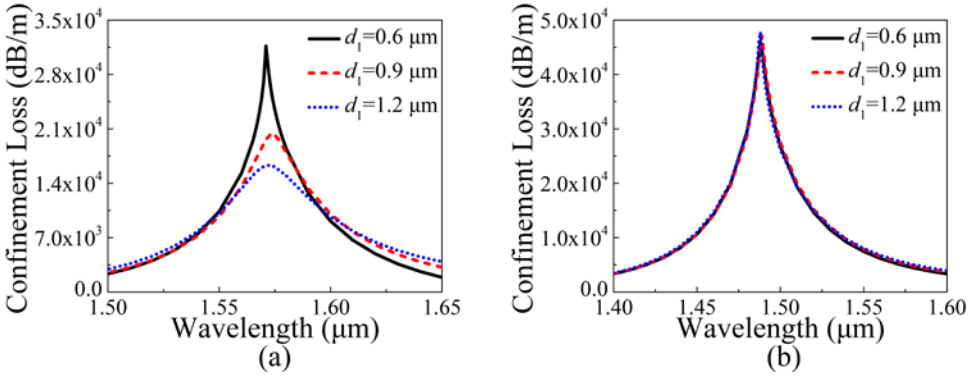

Fig. 5 The confinement losses of **(a)** X-polarization and **(b)** Y-polarization core modes for different d_1.

Figs. 5(a) and 5(b) show the confinement losses of the X-polarization and Y-polarization core modes of the V-shape PCF polarization filter with different d_1, respectively. With the increase of d_1, Re(n_{eff}) of the core mode and second-order SPP mode are almost unchanged. From Fig. 5(a), the two modes along the X-polarization direction change from the complete to incomplete coupling, the resonance wavelength of the X-polarization core mode slightly red-shifts first and then slightly blue-shifts and the peak loss decreases. The two modes along the Y-polarization direction remain the complete coupling, and the resonance wavelength and the peak loss remain almost unchanged.

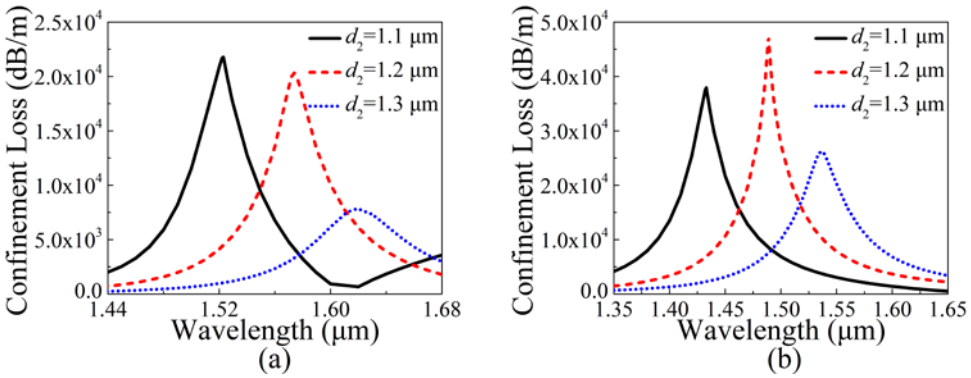

Fig. 6 The confinement losses of **(a)** X-polarization and **(b)** Y-polarization core mode for different d_2.

Figs. 6(a) and 6(b) show the confinement losses of the X-polarization and Y-polarization core

modes of the V-shape PCF polarization filter with different d_2, respectively. With the increase of d_2, Re(n_{eff}) of the core mode decreases, and Re(n_{eff}) of the second-order SPP mode increases. From Figs. 6(a) and 6(b), Both the two modes along the X-polarization and Y-polarization directions change from the complete to incomplete coupling, and the resonance wavelengths of the X-polarization and Y-polarization core modes occur to red-shift. The peak loss of X-polarization core mode continuously decreases, but the peak loss of Y-polarization core mode increases first and then decreases.

Figs. 7(a) and 7(b) show the confinement losses of the X-polarization and Y-polarization core modes of the V-shape PCF polarization filter with different d_3, respectively. With the increase of d_3, Re(n_{eff}) of the core mode decreases, and Re(n_{eff}) of the second-order SPP mode remains almost unchanged. The two modes along the X-polarization direction change from the incomplete to complete coupling. On the contrary, the two modes along the Y-polarization direction change from the complete to incomplete coupling. The resonant wavelengths of the X-polarization and Y-polarization core modes occur to red-shift, but the peak loss of the X-polarization core mode continuously increases, while the peak loss of the Y-polarization core mode increases first and then decreases.

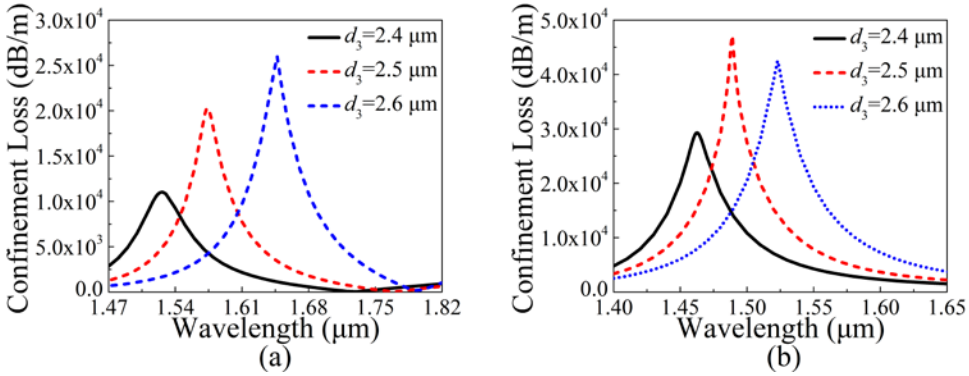

Fig. 7 The confinement losses of **(a)** X-polarization and **(b)** Y-polarization core mode for different d_3.

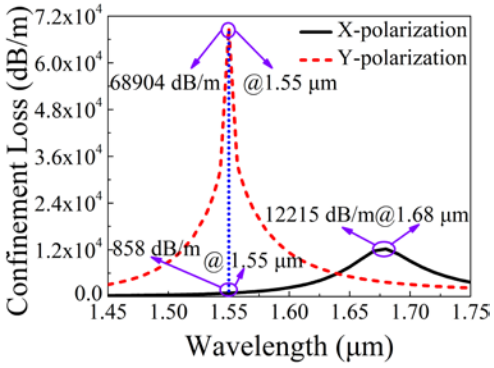

Fig. 8 The confinement losses of the X-polarization and Y-polarization core modes as functions of wavelength.

Based on the above results and coupled-mode theory, the confinement loss increases first and then decreases when the polarization modes change from the incomplete to complete coupling. For this case, there is a critical value for the maximum confinement loss. Moreover, the resonance wavelength and peak loss are affected by the PCF structure parameters. Thus, the optimized structure parameters obtained are as following: Λ=2.1 μm, d_1=0.95 μm, d_2=1.3 μm, d_3=2.53 μm, and t=52.6 nm. At this time, the relationships between the confinement losses of the

X-polarization and Y-polarization core modes and wavelength are shown in Fig. 8. The maximum of the X-polarization core mode at resonance wavelength 1680 nm is 12215 dB/m. The maximum of the Y-polarization core mode at resonance wavelength 1550 nm can be up to 68904 dB/m, but the confinement loss of the X-polarization core mode is as low as 858 dB/m. Therefore, when optical wave centered at 1550 nm are propagated inside the PCF, good filtering effect can be achieved.

The extinction ratio is an important parameter for evaluating the performance of the polarization filter. The wavelength range corresponding to extinction ratio below -20 dB is defined as the bandwidth of the polarization filter. Extinction ratio can be calculated by the equation[24]

$$ER = 10\log_{10}\frac{P_{out}(x)}{P_{out}(y)}, \tag{3}$$

where P_{out} (x) and P_{out} (y) represent the output powers from the X-polarization and Y-polarization directions, respectively.

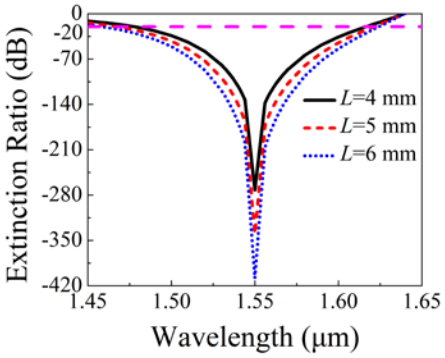

Fig. 9 The extinction ratio as a function of wavelength for different PCF length L.

Table 1 Comparison with the reported PCF polarization filters.

Ref.	Resonance wavelength	The value of the loss peak	Bandwidth of ER below -20 dB	The way to achieve SPP	Optical Fiber Structure
[13]	1311 nm	50800 dB/m	Not mentioned	gold-coated liquid-filled	hexagonl attice
[14]	1550 nm	53600 dB/m	Not mentioned	gold-coated liquid-filled	hexagon lattice
[15]	1310 nm	50000 dB/m	Not mentioned	gold-silver	hexagon lattice
[16]	1550 nm	65700 dB/m	100 nm	gold-coated	hexagon lattice
[22]	1550 nm	43365 dB/m	150 nm	gold-coated	rectangular lattice
This work	1550 nm	68904 dB/m	138 nm	gold-coated	V-shape

The relationships between the extinction ratio and wavelength under different PCF length L are shown in Fig. 9. From Fig. 9, the extinction ratio is decreased as L is increased. When L is chosen as 4 mm, the minimum extinction ratio is -272 dB, and wavelength range corresponding to extinction ratio below -20 dB is from 1478 to 1616 nm, which covers the entire C wave-band and part of S+L wave-band. When L is 6 mm, the maximum extinction ratio reaches -408 dB, and wavelength range corresponding to extinction ratio below -20 dB is from 1459 to 1624 nm, which covers the entire S+C+L wave-band. Thus the bandwidth of the polarization filter is inversely

proportional to L.

In Table 1, the proposed polarization filter is compared with the reported results. By comparison, the peak loss of the proposed polarization filter is highest. Although the bandwidth is slightly smaller than that reported in Ref. [22], it is much easier to fabricate the proposed PCF compared to the PCF with a rectangular lattice.

4. Error-Tolerant Rate Analysis

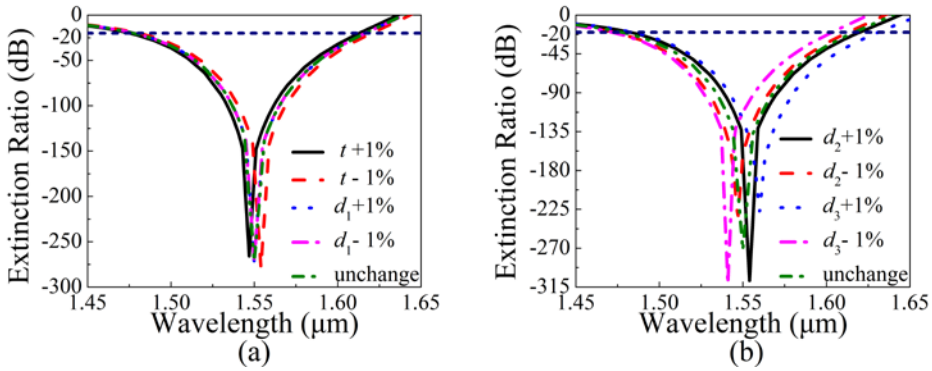

Fig. 10. The extinction ratio when structure parameters **(a)** t , d_1 and **(b)** d_2 , d_3 have deviations of ±1%.

Table 2 The influences of structure parameters on the performances of the V-shape PCF polarization filter (t , d_1, d_2 , and d_3 have deviations of ±1%, L=4 mm)

Parameter change	Resonant wavelength	Y-pol L_C	X-pol L_C	Y-pol/X-pol L_C	Min ER	Bandwidth of ER below -20 dB
unchange	1550 nm	68904 dB/m	858 dB/m	80 times	-272 dB	138 nm
t change +1%	1547 nm	67319 dB/m	852 dB/m	79 times	-266 dB	136 nm
t change -1%	1554 nm	70650 dB/m	874 dB/m	81 times	-279 dB	139 nm
d_1 change +1%	1550 nm	69075 dB/m	853 dB/m	81 times	-273 dB	138 nm
d_1 change -1%	1550 nm	68852 dB/m	860 dB/m	80 times	-272 dB	138 nm
d_2 change +1%	1554nm	77711 dB/m	808 dB/m	96 times	-308 dB	136 nm
d_2 change -1%	1547 nm	59915 dB/m	926 dB/m	65 times	-236 dB	139 nm
d_3 change +1%	1560 nm	57769 dB/m	833 dB/m	70 times	-228 dB	145 nm
d_3 change -1%	1541 nm	78705 dB/m	883 dB/m	89 times	-311 dB	130 nm

The designed V-shape PCF polarization filter can be fabricated by the improved stack and draw method[25,26]. First, the high purity silica rod and tube are drawn into some rods and capillaries respectively. Second, the preform is fabricated according to the designed V-shape PCF structure. Third, the preform is drawn into the PCF. Finally, the gold coating process can be completed by high pressure chemical vapor deposition, magnetron sputtering, or supersonic laser deposition.

Because the slight structure deformation may occur during the fabrication, the variations of extinction ratio are shown in Figs. 10(a) and 10(b) when structure parameters including t, d_1, d_2,

and d_3 have deviations of ±1%. From the Table 2, the minimum bandwidth of extinction ratio below - 20 dB is 130 nm, and good filtering effect can be still achieved, indicating that the designed V-shape PCF polarization filter has excellent error-tolerant rate.

5. Conclusion

In summary, a V-shape PCF polarization filter which operates at 1550 nm is proposed. The complete coupling between the core mode and second-order SPP mode along the Y-polarization direction leads to strong resonance peak. The strongest resonance strength of the Y-polarization core mode can reach 68904 dB/m at the resonance wavelength 1550 nm, where the confinement loss of the X-polarization core mode is as low as 858 dB/m. When the PCF length used is 4 mm, the minimum extinction ratio reaches -272 dB and the bandwidth of extinction ratio below -20 dB is 138 nm, covering the entire C wave-band and part of S+L wave-band. Because the designed V-shape PCF polarization filter has the advantages, including short fiber length, high extinction ratio, wide filter bandwidth, and good error-tolerant rate, it can find important applications in optical communication and sensing systems.

Acknowledgements

This work was supported in part by the National Natural Science Foundation of China (Granted Nos. 61875238), and Fund of State Key Laboratory of Information Photonics and Optical Communications (BUPT) P. R. China (Granted Nos. IPOC2017ZZ05).

References

[1] J. C. Knight, T. A. Birks, P. St. J. Russell, D. M. Atkin, All-Silica Single-Mode Optical Fiber with Photonic Crystal Cladding, Opt. Lett. 21 (1996) 1547-1549.

[2] T. A. Birks, J. C. Knight, P. St. J. Russell, Endless Single-Mode Photonic Crystal Fiber, Opt. Lett. 22 (1997) 961-963.

[3] A. Otto, Excitation of nonradiative surface plasma waves in silver by the method of frustrated total reflection, Zeitschrift für Physik A Hadrons and nuclei 216 (1968) 398-410.

[4] H. Liu, H. R. Wang, W. Zhang, C. C. Chen, Q. Wang, Y. Ding, S. F. Tang, High Sensitive Methane Sensor With Temperature Compensation Based on Selectively Liquid-Infiltrated Photonic Crystal Fibers, Photonic Sens. 9 (2019) 213-222.

[5] B. Y. Li, Z. C. Sheng, M. Wu, X. Y. Liu, G. Y. Zhou, J. T. Liu, Z. Y. Hou, C. M. Xia, Sensitive real-time monitoring of refractive indices and components using a microstructure optical fiber microfluidic sensor, Opt. Lett. 43 (2018) 5070-5073.

[6] T. S. Wu, Y. Shao, Y. Wang, S. Q. Cao, W. P. Cao, F. Zhang, C. R. Liao, J. He, Y. J. Huang, M. X. Hou, Y. P. Wang, Surface plasmon resonance biosensor based on gold-coated side-polished hexagonal structure photonic crystal fibe, Opt. Express 25(2017) 20313-20322.

[7] X. Zhan, R. Wang, F. M. Cox, B. T. Kuhlmey, M. C. J. Large, Selective coating of holes in microstructured optical fiber and its application to in-fiber absorptive polarizers, Opt. Express 15(2007) 16270-16278.

[8] M. A. Schmidt, L. N. P. Sempere, H. K. Tyagi, G. Poulton, P. St. J. Russel, Waveguiding and plasmon resonances in two-dimensional photonic lattices of gold and silver nanowires, Phys. Rev. B 77 (2008) 033417.

[9] H. W. Lee, M. A. Schmidt, H. K. Tyagi, L. P. Sempere, P. St. J. Russel, Polarization-dependent coupling to plasmon modes on submicron gold wire in photonic crystal fiber, Appl. Phys. Lett. 93 (2008) 111102.

[10] H. Liu, C. H. Zhu, Y. Wang, C. Tan, H. W. Li, Polarization-dependent transverse-stress sensing characters of the

goldcoated and liquid crystal filled photonic crystal fiber based on Surface Plasmon Resonance, Opt. Fiber Technol. 41 (2018) 27-33.

[11] A. Khaleque, H. T. Hattori, Polarizer based upon a plasmonic resonant thin layer on a squeezed photonic crystal fiber, Appl. Optics 54 (2015) 2543-2549.

[12] X. C. Yang, Y. Lu, B. L. Liu, J. Q. Yao, Design of a Tunable Single-Polarization Photonic Crystal Fiber Filter With Silver-Coated and Liquid-Filled Air Holes, IEEE Photon. J. 9 (2017) 7105108.

[13] J. R. Xue, S. G. Li, Y. Z. Xiao, W. Qin, X. J. Xin, X, P. Zhu, Polarization filter characters of the gold-coated and the liquid filled photonic crystal fiber based on surface plasmon resonance, Opt. Express 21 (2013) 13733-13740.

[14] L. H. Jiang, Y. Zheng, L. T. Hou, K. Zheng, J. Y. Peng, Surface plasmon induced polarization filter of the gold-coated photonic crystal fiber with a liquid core, Opt. Fiber Technol. 23 (2015) 42-47.

[15] X. C. Yang, Y. Lu, B. L. Liu, J. Q. Yao, Polarization Characteristics of High-Birefringence Photonic Crystal Fiber Selectively Coated with Silver Layers, Plasmonics 13 (2018) 1035-1042.

[16] X. Zhou, S. G. Li, T. L. Cheng, G. W. An, Design of offset core photonic crystal fiber filter based on surface plasmon resonance, Opt. Quant. Electron. 50 (2018) 157.

[17] A. M. Heikal, F. F. K. Hussain, M. F. O. Hameed, S. S. A. Obayya, Efficient Polarization Filter Design Based on Plasmonic Photonic Crystal Fiber, J. Light. Technol. 33 (2015) 2868-2875.

[18] M. S. Islam, J. Sultana, A. A. Rifat, R. Ahmed, A. Dinovitser, B. W.-H. NG, H. EBENDORFF-HEIDEPRIEM, D. Abbott, Dual-polarized highly sensitive plasmonic sensor in the visible to near-IR spectrum, Opt. Express 26 (2018) 30347-30361.

[19] Q. Liu, S. G. Li, H. L. Chen, Two Kinds of Polarization Filter Based on Photonic Crystal Fiber With Nanoscale Gold Film, IEEE Photon. J. 7 (2015) 2700210.

[20] K. Saitoh, M. Koshiba, Full-Vectorial Finite Element Beam Propagation Method with Perfectly Matched Layers for Anisotropic Optical Waveguides, J. Light. Technol. 19 (2001) 405-413.

[21] K. Saitoh, M. Koshiba, Full-Vectorial Imaginary-Distance Beam Propagation Method Based on a Finite Element Scheme: Application to Photonic Crystal Fibers, IEEE J. Quantum Elect. 38 (2002) 927-933.

[22] M. Shi, S. G. Li, H. L. Chen, G. Y. Wang, Y. Y. Zhao, Surface plasmon resonance effect induced tunable polarization filter based on gold film selectively coated photonic crystal fiber, Opt. Commun. 396 (2017) 257-260.

[23] Z. H. Zhang, Y. F. Shi, B. M. Bian, J. Lu, Dependence of leaky mode coupling on loss in photonic crystal fiber with hybrid cladding, Opt. Express 16 (2008) 1915-1922.

[24] L. H. Jiang, Y. Zheng, J. J. Yang, L. T. Hou, Z. H. Li, X. T. Zhao, An Ultra-broadband Single Polarization Filter Based on Plasmonic Photonic Crystal Fiber with a Liquid Crystal Core, Plasmonics 12 (2017) 411-417.

[25] B. Y. Li, M. Wu, X. Y. Liu, G. Y. Zhou, J. T. Liu, Z. Y. Hou, C. M. Xia, Surface Plasmon Resonance on the V-Type Microstructured Optical Fiber Embedded with Dual Copper Wires, Plasmonics 14 (2019) 383-387.

[26] Y. Wang, Q. Huang, W. J. Zhu, M. H. Yang, E. Lewis, Novel optical fiber SPR temperature sensor based on MMF-PCF-MMF structure and gold-PDMS film, Opt. Express 26 (2018) 1910-1917.